Antiferromagnetic ordering in arrays of superconducting π-rings

J. R. Kirtley,[1] C. C. Tsuei,[1] Ariando,[2] H. J. H. Smilde,[2] and H. Hilgenkamp[2]
[1]*IBM Watson Research Center, Yorktown Heights, New York 10598, USA*
[2]*Low Temperature Division, Faculty of Science and Technology and MESA+ Research Institute, University of Twente, Enschede, The Netherlands*

(Received 9 March 2005; revised manuscript received 1 November 2005; published 28 December 2005)

We report experiments in which continuous $YBa_2Cu_3O_{7-\delta}$-Nb junctions with internal sign changes in the Josephson coupling, as well as one-dimensional (1D) and two-dimensional (2D) arrays of $YBa_2Cu_3O_{7-\delta}$-Nb π-rings, are cooled through the superconducting transition temperature of the Nb in various magnetic fields. These systems have degenerate ground states with either clockwise or counter-clockwise spontaneous circulating supercurrents. The final flux state of each facet corner in the junctions and each ring in the arrays was determined using scanning superconducting quantum interference device (SQUID) microscopy. In the continuous junctions, fabricated with facets alternating between alignment parallel to a [100] axis of the YBCO and rotated 90° to that axis, half-fluxon Josephson vortices order strongly into an arrangement with alternating signs of their magnetic flux. We demonstrate that this ordering is driven by phase coupling and model the cooling process with a numerical solution of the Sine-Gordon equation. The 2D ring arrays couple to each other through the magnetic flux generated by the spontaneous supercurrents. Using π-rings for the 2D flux coupling experiments eliminates one source of static disorder seen in similar experiments using conventional superconducting rings [Davidovic *et al.*, Phys. Rev. Lett. **76**, 815 (1996)], since π-rings have doubly degenerate ground states in the absence of an applied field. Although anti-ferromagnetic ordering occurs, with larger negative bond orders than previously reported for arrays of conventional rings, ordering over more than a few lattice spacings is never observed in the 2D arrays, even in geometries without geometric frustration. Monte Carlo simulations of the 2D array cooling process are presented and compared with the experiment.

DOI: 10.1103/PhysRevB.72.214521 PACS number(s): 74.50.+r, 73.40.Gk, 73.40.Rw, 74.72.−h

I. INTRODUCTION

In superconducting rings, the requirement of a single-valued, macroscopic quantum mechanical wave function, combined with the intimate relation between the quantum mechanical phase and the vector potential, results in flux quantization.[2,3] Under the appropriate conditions, two of the flux quantized states can become degenerate, characterized by time-reversed, persistent supercurrents circulating in a clockwise and counter-clockwise direction. These macroscopic circulating currents can be thought of as an analog to an electronic spin. Much work has concentrated on connected superconducting networks, which are an analog of the 2D *XY* spin system.[4,5] In pioneering work, Davidovic *et al.*[1,6] showed that arrays of electrically isolated superconducting rings are an analog of the Ising spin model. Superconducting rings are similar to the Ising spin model since they can have doubly degenerate ground states that interact anti-ferromagnetically upon cooling. However, there are also differences between their physical behavior and the model originally proposed by Lenz[7] and Ising:[8] In the Lenz-Ising model only nearest neighbor interactions are included, while in superconducting rings the ring-ring interaction falls off like $1/r^3$, where r is the spacing between rings. Furthermore, in the original Lenz-Ising model there is no energy barrier to spin flips aside from the spin-spin interaction energy, whereas in superconducting rings the spin flip energy barrier is typically larger than the spin-spin interaction energy, both vary with temperature, and they have in general different temperature dependences.

The Davidovic arrays never showed anti-ferromagnetic ordering beyond a few lattice sites.[1,6] They speculated that one reason for this lack of ordering is that, for there to be two degenerate states, such rings must be cooled in a field equivalent to a half-integer multiple of the superconducting flux quantum $\Phi_0=h/2e$ per ring. Therefore, variations in the lithographically patterned areas of these rings result in different fluxes through different rings in the same field, causing disorder. Superconducting π-rings have an intrinsic phase shift of π in the absence of an externally applied field or supercurrent.[9–11] Such rings have a doubly degenerate ground state in zero applied flux, should not have this source of disorder, and may therefore be a more ideal physical analog to the Ising spin model.

However, use of π-rings for an analog spin system requires a large number of rings. The first superconducting π-rings,[12–15] which depended on the momentum dependence of the pairing wave function in the high-T_c cuprate perovskite superconductors, were made using technologies which would be difficult to extend to many devices. Recently a technology that allows for photolithographic fabrication of π-shift devices and arrays of great complexity, using $YBa_2Cu_3O_{7-\delta}$-Au-Nb (YBCO-Au-Nb) ramp-edge tunneling junctions has been demonstrated.[16,17] Moreover, it has recently been demonstrated that π-rings can also be fabricated using Josephson junctions with ferromagnetic layers in the tunnel barriers.[18–20] In this paper we report on experiments in which the YBCO ramp-edge technology was used to fabricate large arrays of π-rings. A first report on work with similar arrays appeared in Ref. 21. The arrays were cooled in various magnetic fields, and the final "spin" states of the arrays were determined with scanning SQUID microscopy. Anti-parallel ordering of the half-flux quantum vortices was

observed over many facet corners in the continuous facetted junctions. Although stronger anti-ferromagnetic (AFM) correlations were observed in our 2D π-ring arrays than were reported previously for the conventional (O-ring) arrays, in neither case did AFM ordering extend beyond a few lattice sites. Although using π-rings eliminated one source of disorder, inhomogeneous flux biasing due to the applied fields required for O-rings, there are other sources of disorder, including inhomogeneities in the ring critical currents and critical temperatures, and nonuniform cooling rates. We will discuss the influences of these sources on our results, as well as dynamic effects, using Monte Carlo modeling of the cooling process.

II. EXPERIMENTAL METHODS

Various samples consisting of continuous facetted junctions and one- and two-dimensional π-ring arrays have been realized using ramp-type $YBa_2Cu_3O_{7-\delta}$-Au-Nb Josephson contacts. The fabrication of ramp-type $YBa_2Cu_3O_{7-\delta}$-Au-Nb Josephson junctions has been described previously in detail in Refs. 16 and 17. In short, the samples were prepared by first epitaxially growing a bilayer of [001]-oriented $YBa_2Cu_3O_{7-\delta}$ and $SrTiO_3$ by pulsed-laser deposition on [001]-oriented $SrTiO_3$ single crystal substrates. For the 1D array samples a 150 nm $YBa_2Cu_3O_{7-\delta}$ and a 100 nm $SrTiO_3$ film were used, while for the 2D array samples a 340 nm $YBa_2Cu_3O_{7-\delta}$ and a 67 nm $SrTiO_3$ film were used. In these bilayers the basic layout of the structures, which will be described below in more detail, is defined by photolithography and Ar ion milling. This process results in interfaces with a slope of 15–35° with respect to the substrate, which provides access to the *ab*-planes of the $YBa_2Cu_3O_{7-\delta}$ and allows the exploitation of *d*-wave phase effects. Special care is taken to align all interfaces accurately along one of the $YBa_2Cu_3O_{7-\delta}$ [100] axes. After etching the ramp and cleaning of the sample, a 7 nm $YBa_2Cu_3O_{7-\delta}$ interlayer is deposited, the function and properties of which are described in Ref. 17, followed by the *in situ* pulsed-laser deposition of a Au barrier-layer of 12 nm for the 1D array samples and 20 nm for the 2D array samples. A 160 nm Nb counter electrode is then formed by dc sputtering and structured by lift-off. Each chip contained several reference-junctions. At $T=4.2$ K, these showed a typical critical current per micrometer junction-width $I_c/w \approx 0.10$ mA/μm for the 1D array samples and $I_c/w \approx 0.18$ mA/μm for the 2D array samples. From these, a value for the Josephson penetration depth $\lambda_j \approx 1$ μm ($T=4.2$ K) for all samples is deduced, which is the characteristic length scale over which Josephson vortices (fluxons) extend.

The sample magnetic fields were imaged with a high resolution scanning SQUID microscope.[22–25] The SQUID microscope images shown here were made at a temperature of $T < 5$ K, with the sample cooled and imaged in the same fields. The size of the pickup loop used will be indicated for each image. The samples were warmed through the superconducting critical temperature of the Nb and cooled at controlled rates either using a noninductive heater, or by passing warm ^{4}He gas past the sample, with the SQUID pickup loop 2 mm above the sample plane. The SQUID substrate was then brought into contact with the sample for imaging. In all of the images presented here, we determined that the SQUID was not causing spin flips of the rings during imaging by repeated scanning of the same area.

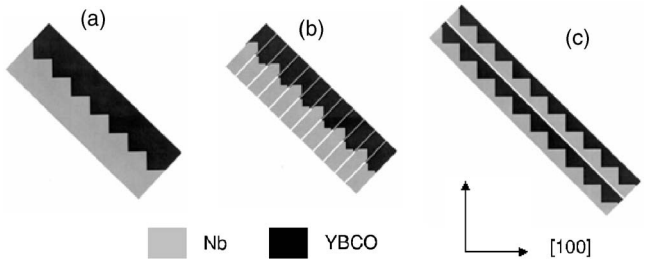

FIG. 1. Schematics of the 3 types of facetted junctions studied in this work. (a) A continuous, single facetted junction. (b) Junction with the individual half-fluxons electrically isolated from one another. (c) Double row of continuous facetted junctions.

A first configuration for which the generation and coupling of half-integer flux quanta was investigated is the continuous facetted junction,[16] several instances of which are shown schematically in Fig. 1. In these structures, the *d*-wave order parameter of the $YBa_2Cu_3O_{7-\delta}$ induces a difference of π in the Josephson phase-shift ϕ across the $YBa_2Cu_3O_{7-\delta}$-Au-Nb barrier for neighboring facets. For facet lengths a in the wide limit, i.e., $a \gg \lambda_j$, the lowest-energy ground state of the system is expected to be characterized by a spontaneous generation of a half-integer flux-quantum at each corner. This half-fluxon provides a further π-phase change between neighboring facets, either adding or subtracting to the *d*-wave induced π-phase shift, depending on the half-flux quantum polarity. In both cases this leads to a lowering of the Josephson coupling energy across the barrier, as this energy is proportional to $(1-\cos\phi)$. We studied three types of facetted junctions. The first [Fig. 1(a)] was an isolated, continuous junction with many adjacent facets. The second [Fig. 1(b)] was lithographically patterned to electrically isolate each half-fluxon from its neighbor. The final type [Fig. 1(c)] had two continuous facetted junctions close together, but electrically isolated from one another, to test for field coupling between continuous facetted junctions.

The two-dimensional π-ring arrays were made up of individual rings patterned as indicated schematically in Fig. 2. There were two types of rings, square [Fig. 2(a)] and hexagonal [Fig. 2(b)]. The rings were patterned into arrays with four different geometries, as shown in the scanning electron microscopy images of Fig. 3. In all cases the nearest-neighbor distances in these arrays was 11.5 μm center to center. The details of the ring geometries, critical currents, self-inductances, and mutual-inductances are given in Table I.

III. RESULTS

Figure 4 shows representative scanning SQUID microscope images of 6 zigzag $0-\pi$ facet junctions. All of these images were of samples on the same substrate, and imaged in the same cooldown in nominal zero field (<0.5 μT) at

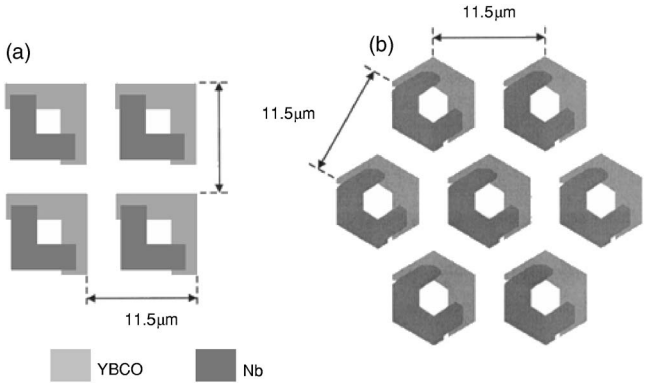

FIG. 2. Schematic diagram of two types of π-rings used for the 2D arrays reported in this paper. Type (a) was used in the square arrays, and type (b) was used in the triangular, honeycomb, and kagomé arrays.

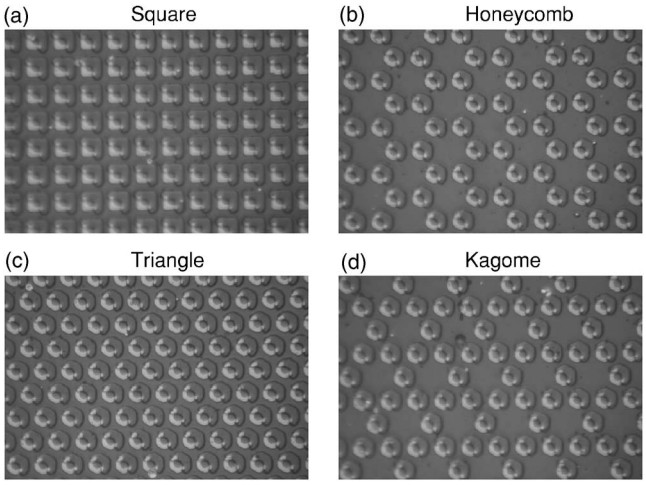

FIG. 3. Scanning electron microscopy images of 4 arrays of π-rings, with 2.7 μm junctions and 11.5 μm ring to ring spacings.

T=4.2 K. In all three types of facetted junctions, half-fluxon Josephson vortices were spontaneously generated at the points where the facets met, as expected. When the continuous facetted junctions [Fig. 1(a)] were cooled in zero field through the niobium superconducting transition temperature, the signs of the half-fluxons strongly tended towards perfect anti-parallel ordering, in which the persistent supercurrents alternated between clock-wise and counter clock-wise flow [Figs. 4(a) and 4(d)–4(f)]. There are two possible mechanisms for this ordering. In the first, ordering is driven by the minimization of the total junction Josephson coupling energy during the cooling process. We refer to this as "phase" coupling, because the Josephson currents and energies are determined by the difference in superconducting phase across the junction ϕ. In the second, the anti-ferromagnetic ordering is driven by a minimization of the total magnetic field energy in the junction and its environment. We refer to this as "field" coupling. In order to determine the relative strengths of these mechanisms, facetted junctions were fabricated with each half-fluxon electrically isolated from its neighbor [Fig. 1(b)]. This should eliminate the phase coupling mechanism. Indeed, when this is done the anti-parallel ordering is much weaker. Two examples are shown in Figs. 4(b) and 4(c). In Fig. 4(b) the half-fluxons all have the same orientation. We believe that this is because they align with a small residual field. Figure 4(c) shows a more random alignment of the isolated half-fluxons.

In order to test for magnetic field coupling between the chains of half-fluxons in the continuous junctions, double facetted junctions [Fig. 1(c)] were also fabricated and tested. It appeared that also in this case the phase coupling was stronger than the field coupling: Figure 4(d) shows a section of a 40 μm facet double junction that shows in-phase alignment between the two anti-parallel ordered half-fluxon chains. Because this arrangement places the positive half-fluxons in the lower left chain closest to the negative half-fluxons in the upper right chain, this is the lowest energy arrangement. However, in sections of the 1D chains which show defects, as in the center of the upper right chains in

TABLE I. Details of 2D lattice samples; critical current density is $J_c \approx 5 \times 10^8$ A/m^2.

	Square	Triangular	Honeycomb	Kagomé
height YBCO (nm)	340	340	340	340
height STO (nm)	67	67	67	67
height Nb (nm)	160	160	160	160
width JJ 1 (μm)[a]	2.75	2.70	2.70	2.70
width JJ 2 (μm)[b]	2.75	3.75	3.75	3.75
hole (μm)	2.50	~3.10	~3.10	~3.10
self-inductance (pH)[b]	3.93	~3.90	~3.90	~3.90
self-inductance (pH)[c]	4.57	—	—	—
nearest neighbor distance (μm)	11.5	11.5	11.5	11.5
nearest neighbor mutual (pH)[c]	0.025	—	—	—

[a]Designed value.
[b]Estimate with standard formulas.
[c]Estimate using FastHenry, λ_{YBCO}=160 nm and λ_{Nb}=40 nm.

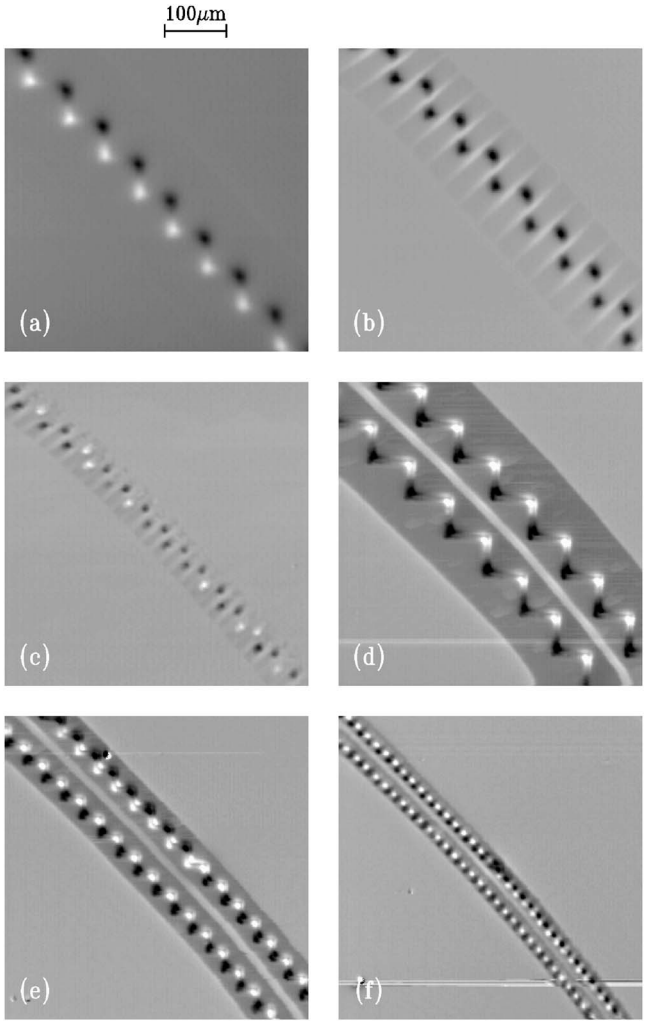

FIG. 4. Scanning SQUID microscope images of continuous facetted YBCO-Au-Nb $0-\pi$ junctions, cooled in nominally zero field, and imaged with a 4 μm diameter pickup loop. (a) Continuous junction with 40 μm facet lengths. (b) Electrically disconnected junction with 40 μm between facet corners. (c) Electrically disconnected junction with 20 μm between facet corners. Two parallel facetted $0-\pi$ junctions with 40 μm (d), 20 μm (e), and 10 μm (f) between facet corners. The apparent curvature of the junctions in these images is an artifact of the scanning mechanism.

Figs. 4(e) and 4(f), the interchain alignment goes from in-phase to out-of-phase when the interchain ordering has a defect, but one chain does not develop a second defect to align the interchain spins. Therefore, it appears that the energy cost to create a defect is larger than the energy gain from making neighboring chains in-phase.

When the facetted junctions are cooled in an externally applied magnetic field, one spin direction becomes energetically favored over the other, but there is a competition between this energy and the anti-parallel coupling energy during the cooling process. An example is shown in Fig. 5. More detailed results and modeling of this facetted junction will be described in the next section.

In the electrically disconnected 2D lattices of Fig. 3, the square and honeycomb arrays are geometrically unfrustrated, as their magnetic moments can be arranged so that all nearest

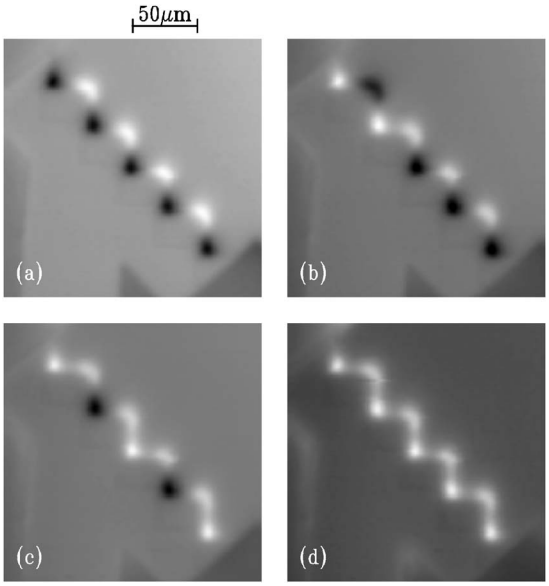

FIG. 5. Scanning SQUID microscope images of a facetted YBCO-Nb $0-\pi$ junction with 10 facets each 40 μm long, cooled in fields of 0 nT (a), 32 nT (b), 74 nT (c), and 110 nT (d), and imaged at 4.8 K with an 8 μm square pickup loop.

neighbors have opposite spins, and the ground state of these lattices are only doubly degenerate. In contrast, the triangle and kagomé lattices are geometrically frustrated, since it is impossible for all of the rings to have all nearest neighbors anti-ferromagnetically aligned, and the ground states are highly degenerate. Figure 6 shows examples of scanning SQUID microscope images of the arrays of Fig. 3 after cooling in nominally zero field. Although regions of anti-ferromagnetic ordering are seen in the unfrustrated arrays [Figs. 6(a) and 6(b)], anti-ferromagnetic ordering beyond a few lattice distances was never observed. Nevertheless, anti-ferromagnetic correlations were seen in all the 2D π-ring arrays. A measure of the short range antiferromagnetic correlations[26,27] is the bond order

$$\sigma = 1 - \frac{x_{AF}}{2x_+x_-}, \tag{1}$$

where x_{AF} is the fraction of the nearest neighbor pairs with opposite supercurrent circulation, and $x_+(x_-)$ is the fraction of rings which have up (down) moments. Perfect antiferromagnetic correlation would correspond to $\sigma=-1$. The minimum possible bond order at zero applied field for the frustrated triangular and kagomé lattices is $\sigma=-1/3$.[28] The images in Fig. 6 are labeled with values for the bond orders.

It is to be expected that the anti-ferromagnetic ordering of the 2D arrays should improve if they are cooled more slowly through the Nb superconducting transition. Figure 7 shows SQUID microscope images of the same region of the honeycomb 2D lattice of Fig. 3, after cooling at various rates. The individual panels are labeled with the cooling rates and final state bond orders. The anti-ferromagnetic ordering increases with slower cooling rates. One question that can be asked is: Do particular regions of the 2D array order more strongly than others? The white circles in Fig. 7 outline the six-

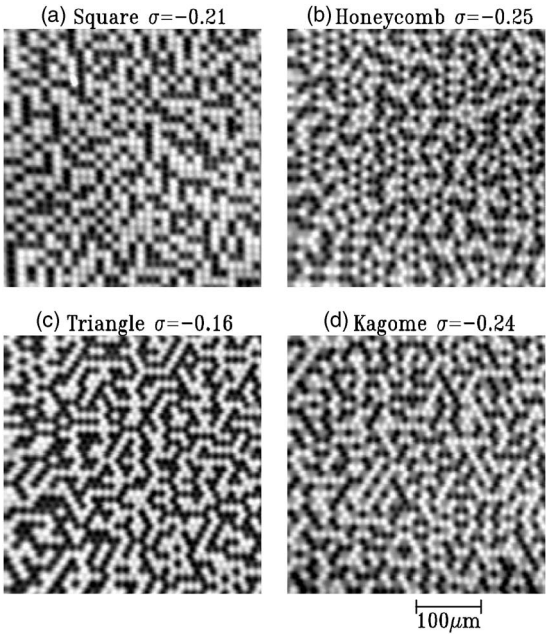

FIG. 6. SQUID microscopy images of four electrically disconnected arrays of π-rings, in the geometries illustrated in Fig. 3, with values for the ring parameters given in Table I. These images were taken at 4.2 K with a 4 μm diameter pickup loop after cooling in nominally zero field at 1–10 mK/s. The spin up fractions x_+ and full scale variations in the scanned SQUID sensor flux ($\Delta\Phi_s$) were $x_+=0.56$, $\Delta\Phi_s=0.12\Phi_0$ for the square lattice; $x_+=0.51$, $\Delta\Phi_s=0.11\Phi_0$ for the honeycomb lattice; $x_+=0.50$, $\Delta\Phi_s=0.10\Phi_0$ for the triangular lattice; and $x_+=0.54$, $\Delta\Phi_s=0.12\Phi_0$ for the Kagome lattice, respectively.

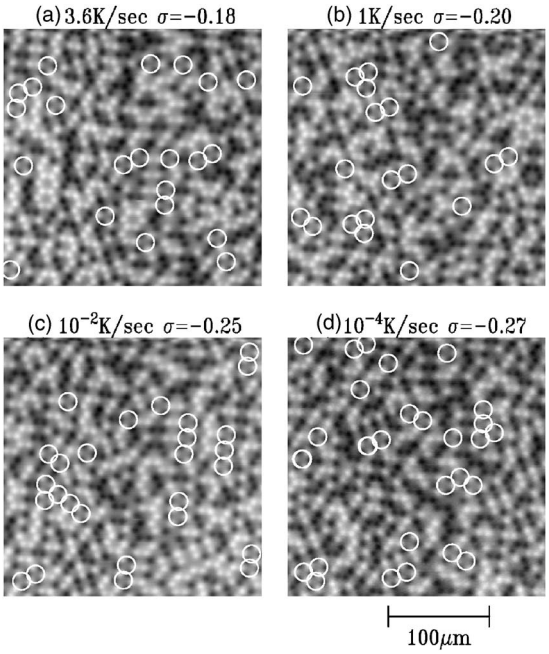

FIG. 7. SQUID microscopy images of a honeycomb array in the geometry illustrated in Fig. 3, cooled in nominally zero field through the Nb superconducting transition temperature at different cooling rates. Each panel is labeled with the cooling rate and experimentally determined bond order σ. The white circles superimposed on the images label 6-ring loops in the honeycomb lattice in which the rings are perfectly anti-ferromagnetically ordered.

member rings in the honeycomb arrays in which all neighbors are anti-ferromagnetically aligned. This provides a convenient way of visualizing regions of local order. It appears that there are no correlations between the positions of the ordered six-member rings from cooldown to cooldown, and we conclude that the ordered regions are randomly distributed in space.

In the O-ring experiments of Davidovic *et al.*[1,6] repeated cooling resulted in a particular ring often being in the same final state (spin-up or spin-down). This is presumably the result of the rings having slightly different effective areas, and therefore cooling in slightly different effective fields, since O-rings must be cooled in finite fields for there to be degenerate states. The individual rings in our 2D π-ring arrays appear to have random final states. Figure 8 shows a difference image between Figs. 7(b) and 7(c), which were taken after successive cooldowns. In this image, the rings which did not switch sign from one cooldown to the next are not visible, the rings which switched from down to up appear black, while the rings which switched from up to down appear white. Of the roughly 663 rings in this field of view, 152 switched from down to up, and 162 switched from up to down. This is consistent with random switching from one cooldown to the next.

IV. MODELING

For the current purposes we treat the facetted ramp edge junction as a linear junction with alternating regions of 0- and π-intrinsic phase shifts $\theta(x)$ extending in the x direction, with the junction normal in the z direction, and the junction width w in the y direction small compared with the Josephson penetration depth $\lambda_J=\sqrt{\hbar/2e\mu_0 d j_c}$, where d is the spacing between the superconducting faces making up the junction, and j_c is the Josephson critical current per area of the junction. The quantum mechanical phase drop $\phi(x)$ across

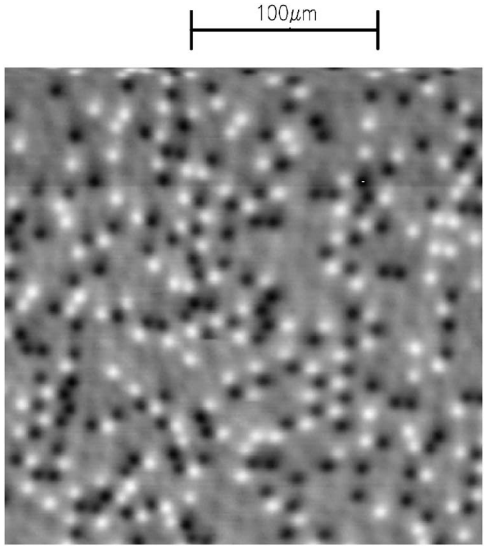

FIG. 8. Difference image obtained from subtracting the image of Fig. 7(c) from Fig. 7(b), to determine which rings flipped sign after successive cooldowns.

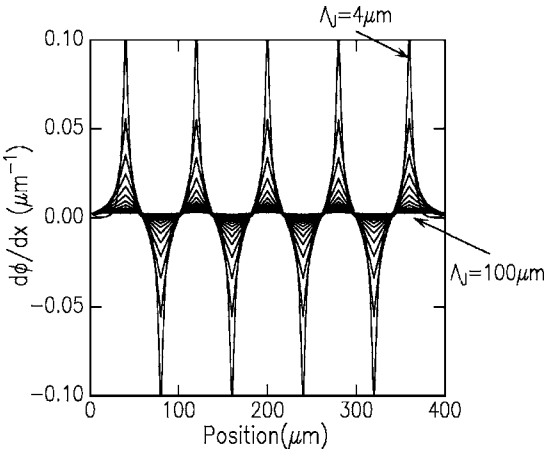

FIG. 9. Modeling of the cooldown of the facetted junction of Fig. 5. The junction has 10 faces, each 40 microns long, with alternating 0- and π-intrinsic phase shifts.

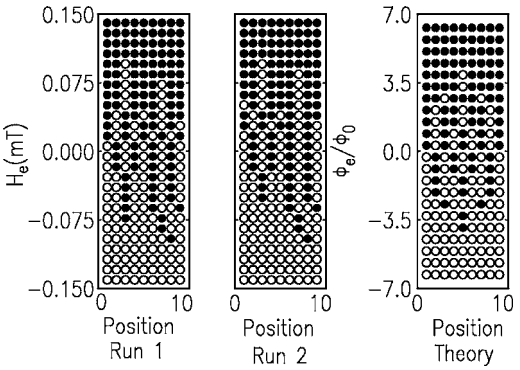

FIG. 10. Results from cooldown of the facetted junction of Fig. 5 in several externally applied magnetic fields. Half-fluxons with magnetic fields in one direction are represented by open symbols, those with the opposite sense with closed symbols. The left two panels are experimental results from two successive runs; the right panel represents modelling as described in the text.

the junction is the solution of the Sine-Gordon equation:

$$\frac{\partial^2 \phi}{\partial x^2} = \frac{1}{\lambda_J^2} \sin(\phi(x) + \theta(x)). \tag{2}$$

Analytical solutions to this equation are available,[29–31] but here we solve Eq. (2) numerically.[32–36] Defining a dimensionless coupling parameter

$$\alpha = \frac{\lambda_J^2}{(\Delta x)^2}, \tag{3}$$

the differential equation, Eq. (2), turns into a difference equation on a grid of size Δx:

$$\phi_{n+1} - 2\phi_n + \phi_{n-1} = \frac{1}{\alpha} \sin(\phi_n + \theta_n). \tag{4}$$

Taking the net current across the junction equal to zero, using a reduced externally applied magnetic field $h_e = 2ed\lambda_J H_e/\hbar$, and using the relation between the gradient of the phase and the field H in the junction:

$$H(x) = \frac{\hbar}{2ed} \frac{\partial \phi}{\partial x}, \tag{5}$$

we find boundary conditions that are described as difference equations, where n_j is the total number of junctions:

$$\phi_{n_j} - \phi_{n_j - 1} = \phi_2 - \phi_1 = \frac{h_e}{\sqrt{\alpha}}. \tag{6}$$

These coupled difference equations are solved using a relaxation method to find the solution $\phi(x)$, iterating to convergence. As the junction cools through the superconducting transition temperature T_c, the supercurrent density j_c increases from zero, so that λ_J decreases from infinity. To model the cooling process, we first solve Eq. (4) for λ_J much larger than the facet length L_f, then decrease λ_J by a small amount, take the previous solution as the starting point for the next solution, and repeat until $\lambda_J \ll L_f$. An example is shown in Fig. 9. Here the externally applied flux was set at $\Phi_e = H_e d L = \Phi_0/2$, the total junction length $L = 400$ μm, $\Delta x = 1$ μm, with 10 facets each of length $L_f = 40$ μm, an initial $\lambda_J = 100$ μm, which was decreased to 4 μm in 24 equal steps. The field threading the junction is given by $H(x) = (\Phi_0/2\pi d) d\phi/dx$. The final solution strongly favors anti-parallel arrangement of the half-fluxon circulating supercurrents.

We can understand why the $0-\pi$ facetted junctions cool into anti-parallel order, while the isolated linear arrays of π-rings do not, by considering the energetics of the cooling process. Written as a difference equation, the free energy for a particular state of the facetted junction becomes:

$$F_V = \frac{\hbar j_c w \Delta x}{2e} \sum_1^{n_j - 1} \left(1 - \cos(\phi_n + \theta_n) + \frac{\alpha}{2} (\phi_{n+1} - \phi_n)^2 \right). \tag{7}$$

Numerical solution of the Sine-Gordon equation as described above for the facetted junction of Fig. 5 shows that the free energy/facet, when the junction is in anti-parallel ordering, is $\sim -5 \times 10^5$ K/$\lambda_J(\mu\text{m})$. The energy cost to form a defect, by flipping one spin, is $\sim 7.2 \times 10^5 e^{-45/\lambda_J(\mu\text{m})}$ K. This implies that when the free energy/facet is comparable to $k_B T$, the energy cost to form a defect is $\approx 7.2 \times 10^5$ K: It is energetically favorable to form anti-ferromagnetic ordering in linear $0-\pi$ facetted junctions cooled in zero field.

Figure 10 compares the results from repeated cooling of the 10-facet zigzag junction under various magnetic fields with modeling using the numerical solution of the sine-Gordon equation outlined above. Note that there are some disorder effects in the cooling process, as evidenced by the slight differences between the two experimental runs. The qualitative features of the data are reproduced by the modeling, although the experimental results are not as symmetric with respect to inversion in position, or with respect to field reversal, as predicted. One possible source of the observed asymmetry might be field gradients. However, putting a linear field gradient into the model did not improve the fit with

experiment. Another source of asymmetry might come from the asymmetry of the junction and lead geometry.

The cooling process is different, and much more interesting, for isolated π-rings than for the continuous facetted junctions. Although there is an enormous literature on the magnetic properties of 2D arrays of interacting spins,[37,38] there are relatively few exactly solvable problems.[39] In the absence of an externally applied magnetic field, and neglecting the influence of neighboring rings on the distribution of circulating supercurrents,[40] our π-rings have only two degenerate states. Therefore, a Lenz-Ising model,[7,8,41] is more appropriate than an XY model, in which the spins are constrained to rotate in a plane, or a Heisenberg model, in which the spins can be oriented isotropically. The Lenz-Ising Hamiltonian is

$$H = \sum_{i,j} J s_i s_j, \tag{8}$$

where the sum is over nearest neighbors, J is positive for an anti-ferromagnetic interaction, $s_i, s_j = \pm 1$ are the system spins, and we have neglected the effect of an externally applied magnetic field for the moment. However, as mentioned in the introduction, the present problem is physically different from traditionally studied Ising problems in two ways. First our 2D π-ring arrays interact through a mutual inductance which falls off like r^{-3}, where r is the spacing between rings. This system should therefore be understood using a model somewhere in between a nearest neighbor Lenz-Ising model and a Kosterlitz-Thouless model[42] where the interactions fall much more slowly, like $\log(1/r)$. We will demonstrate numerically below that our problem can be treated adequately by considering a few shells of nearest neighbors. The second difference from a traditional Lenz-Ising model is that there is a barrier to spin flips, and both the ring-ring coupling energies and the barriers to ring supercurrent reversals are temperature dependent, with in general different temperature dependences for the two energies. The relative complexity of this problem means that it is unlikely that analytical solutions exist. We turn to numerical solutions, in particular Monte Carlo methods,[43,44] in an attempt to understand our results.

In the Metropolis Monte Carlo scheme,[45] suitable for a steady state situation at fixed temperature, a Markov chain is constructed by using the principle of detailed balance: The probability of moving from one state to the next in the Markov chain is proportional to the Boltzmann factor $\exp(-\delta H/k_B T)$, where δH is the change in energy between the two states, k_B is Boltzmann's constant, and T is the temperature. In the dynamic interpretation of the Metropolis scheme, the proportionality constant multiplying the Boltzmann factor can be taken to be the product of an attempt frequency times the Monte Carlo time interval.[43] However, this scheme is not directly applicable to our situation, both because the dynamic interpretation does not necessarily represent the real time evolution of the system,[43] and because in our case there is a finite, and temperature dependent energy barrier to reversal of the ring circulating supercurrents. Creuz has argued that a dynamical system can be modeled by "microcanonical" simulation, which uses a energy reservoir either attached to a mobile "demon,"[46] or associated with each element in the simulation.[47] This allows the simulation to proceed while conserving the total system energy. However, this scheme is not suitable for modeling our cooling process because at each temperature the spins are assigned random initial values consistent with the temperature: There is no system memory of the history of the cooldown. In the present paper we take the ideas of Creutz one step further: Each ring is conceptually weakly attached to a thermal reservoir at a temperature T. The solution to the dynamical problem at each temperature T is taken as the starting point for the solution at a temperature $T-\delta T$. The temperature step δT divided by the time interval δt for simulating each temperature is identified with the experimental cooling rate dT/dt. Each ring has a barrier to supercurrent reversal which depends not only on the critical current and inductance of the ring, but also on the local fields applied by the neighboring rings. In this picture the process of supercurrent reversal is thermally activated. Thermally activated noise processes in SQUIDs are well understood.[48] Our scheme for modeling the cooling process in our rings is to start at a temperature very close to the superconducting transition temperature T_c with all of the π-rings in a spin-up state. Close to T_c both the ring-ring coupling energy E_c and the barrier energy to supercurrent reversal E_b are small, and the ring supercurrents reverse rapidly and at random. As the temperature is lowered, both these energies become larger, and the supercurrent reversal becomes less frequent, but supercurrent reversal from a state with anti-parallel near-neighbor circulations is slightly less likely than supercurrent reversal from a state with parallel near-neighbor circulations. When the barrier energy becomes comparable to $k_B T_c$, the supercurrent directions are "frozen in." Whether the final state is ordered or not depends on the details of the cooling process, such as the temperature dependent ring critical currents, self-inductances, mutual inductances, cooling rate, and array geometry.

We model our isolated π-rings as symmetric (equal junction critical currents) two-junction rings with total inductance L and single junction critical current I_c.[49] A symmetric two-junction π-ring spontaneously generates circulating supercurrent in the absence of an applied field for any value of I_c and L. However, as soon as there is an asymmetry in the junction critical currents, a critical value of the $I_c L$ value must be exceeded for there to be circulating supercurrents.[49] In the limit of very large asymmetries, equivalent to a one-junction ring, the condition $\beta \equiv 2\pi L I_c/\Phi_0 > 1$, where $\Phi_0 = h/2e$ is the superconducting flux quantum, must be satisfied before there are spontaneous circulating supercurrents. We have also modeled the system as one-junction rings, with qualitatively similar results. In this case the turn-on of spontaneous currents is more abrupt and the predicted antiferromagnetic ordering is stronger than in the symmetric two-junction case. The free energy U of a symmetric two-junction π-ring can be written as[49]

$$U = \frac{I_c \Phi_0}{2\pi}\left\{2 - \cos\varphi_1 - \cos\varphi_2 + \frac{1}{2\beta}[\varphi_2 - \varphi_1 + \pi + 2\pi\phi_a]^2\right\}, \tag{9}$$

where φ_1 and φ_2 are the quantum mechanical phase drops across the two junctions, and $\phi_a = \Phi_a/\Phi_0$ is the reduced ap-

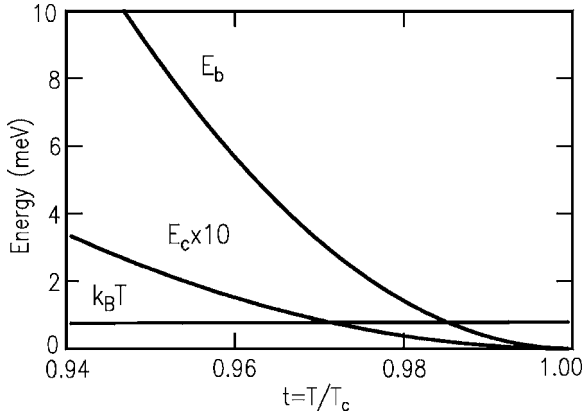

FIG. 11. Calculated energies for the honeycomb ring arrays of Fig. 3 as a function of the reduced temperature. E_b is the barrier to thermally activated flipping of the sign of the spontaneous magnetization, E_c is the strength of the spin-spin coupling energy, and k_BT is the thermal energy.

plied flux. At temperatures important in the cooling process, close to the Nb superconducting transition temperature T_c, field screening effects can be neglected, since the magnetic penetration lengths are larger than the size of the sample. Under these conditions, we estimate the ring self-inductances (for 2.7 μm junction width rings spaced by 11.5 μm) to be $\approx$3.9 pH, and the mutual inductance M between nearest neighbor rings to be $\approx$0.025 pH. The ring ordering process will occur in the regime $\beta \ll 1$ for a symmetric two-junction π-ring array. In this limit, and in the limit $\phi_a \ll 1$, it can be shown that the potential barrier to flipping the sign of the ring supercurrents in the ith ring is approximated by

$$E_{bi} \approx \frac{\beta_i^*}{2}\frac{I_c\Phi_0}{2\pi}, \tag{10}$$

with $\beta_i^* = \beta + 4\pi\Phi_a s_i/\Phi_0$, where $s_i = \pm 1$ is the spin of the ith ring, and

$$\Phi_a = \Phi_e - \sum_j \frac{M_{ij}\Phi_m}{L} s_j, \tag{11}$$

where Φ_e is the externally applied flux and $M_{i,j}$ is the mutual inductance between the ith and jth rings. In the same limits, the value of the spontaneous flux Φ_m generated by the ring is given by

$$\frac{\Phi_m}{\Phi_0} \approx \frac{\beta}{2\pi}. \tag{12}$$

A measure of the spin-spin coupling energy E_c is the difference between the energy barrier for all nearest neighbor spins up, minus that energy barrier if one of the neighbor spins is down. Within these approximations this energy is

$$E_c \approx 2M_{ij}I_c^2 \approx 2M_{ij}I_s^2, \tag{13}$$

where $I_s = \Phi_m/L$ is the spontaneous circulating supercurrent in each ring, and using Eq. (12). Figure 11 plots the calculated barrier to thermally activated flipping E_b, (neglecting for this plot the ring-ring coupling energy), nearest neighbor coupling energy E_c, and the thermal energy k_BT as a function of temperature for the honeycomb ring array of Fig. 6. Both E_b and E_c increase as the temperature is lowered until the flipping freezes out at a temperature T_f such that $E_b/k_BT_f \approx -\ln[\gamma(k_B\nu_0 T_f)^{-1}dT/dt]$, where $\gamma = dE_b(T_f)/dT$,[50] and ν_0 is the attempt frequency (to be described below). For the rings of Fig. 6, this estimate gives $E_b/k_BT_F \approx 8$. Within the approximations above $E_c/E_b \approx 4M_{i,j}/L \approx 0.025$. Therefore, anti-parallel alignment is energetically favored in isolated π-rings, but not nearly as strongly as in continuous facetted junctions.

As the temperature is lowered through T_c, the junction critical currents increase, creating two distinct circulating states. Thermally activated switching between these states has a transition rate[48]

$$r \approx \frac{1}{\pi\beta\tau} e^{-E_{bi}/k_BT}, \tag{14}$$

where $\tau \equiv \Phi_0/2\pi I_c R$ is the junction characteristic time.[48] We take the junction critical current $I_c(0) = 0.55$ mA, $I_c(T) = I_c(0)(1 - T/T_c)$,[51] assume that the self-inductance of the rings is temperature independent, and take $R = 1\Omega$ for the 2D arrays presented in this paper. It is of interest to note that the power dissipated per ring near the "freezout" temperature is of order $k_BT_c/\tau \sim 10^{-11}$ W.

To model the cooling process in our 2D ring arrays we use a Metropolis Monte Carlo[45] simulation as outlined above. A 30×30 element array is set up with the same geometry as the experimental arrays. Boundary effects are minimized by using periodic boundary conditions: Rings at one edge of the array are treated as if their nearest neighbors are the corresponding rings at the opposite edge. The results of our simulations do not depend sensitively on whether periodic or nonperiodic boundary conditions are used.

In order to determine whether our system is dominated by nearest neighbor interactions, we have performed the following model calculation: It is known that for a 2D honeycomb lattice with the Ising Hamiltonian of Eq. (8), the Neel temperature is given by $k_bT_N = 1.52J$ if the sum j is over 1st nearest neighbors. We did the Monte Carlo simulation outlined above, but taking the supercurrent reversal barrier to be $E_{bi} = 2J\Sigma_j s_j (a/r_{ij})^3$, where a is the 1st nearest neighbor spacing, and r_{ij} is the distance between the ith and jth rings, and taking the probability for the ith ring to spin flip per Monte Carlo cycle $P_i = \exp(-E_{bi}/k_BT)$. The results are displayed in Fig. 12. If the sum j is only over the three nearest neighbors, the bond order sigma extrapolates to -1 at $J/k_BT \approx 0.66$, in agreement with expectation. These agreements with analytical results, as well as those represented by the solid lines in Fig. 15, provide confidence in our Monte Carlo simulation. There is a slight "tail" to the data at lower temperatures, which becomes smaller for slower cooling rates. The intercept moves to significantly lower temperatures (higher values of J/k_bT) if the six 2nd nearest neighbors are included. This is to be expected, since the 2nd nearest neighbors have the same supercurrent circulation as the center ring for antiferromagnetic ordering, raising the system energy. The intercept decreases again if 3rd nearest neighbors are included,

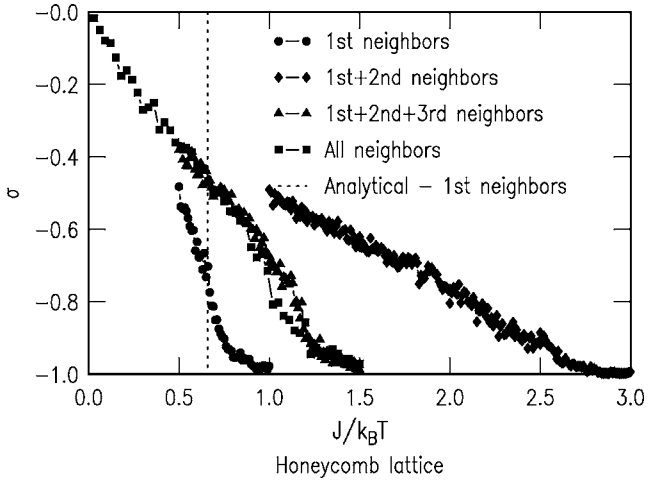

FIG. 12. Bond order as a function of J/k_BT for a honeycomb lattice. In this simulation the barrier to supercurrent reversal was taken to have the form $E_{bi}=2J\Sigma_j s_j(a/r_j)^3$. The sum j was over the three 1st nearest neighbors (circles), also over the six 2nd nearest neighbors (diamonds), also over the three third nearest neighbors (triangles), or over all the rings in the lattice (squares). The dashed line represents the mean-field prediction for the Neel temperature for a 2D honeycomb lattice Ising model, including only nearest neighbor interactions. In this simulation 10^{10} Monte Carlo cycles were taken for each step $\Delta J/k_BT_c=0.01$ for the 1st, 1st+2nd, and 1st+2nd+3rd nearest neighbor shell calculations, and 10^8 steps were taken for each step $\Delta J/k_BT_c=0.02$ for the all neighbors calculation.

but the change is smaller than that involved in including the 2nd nearest neighbors. In fact, the Neel temperature does not change appreciably from the 1st+2nd+3rd nearest neighbor result if all rings in the array are included. We conclude that the ring-ring mutual inductances fall off sufficiently rapidly

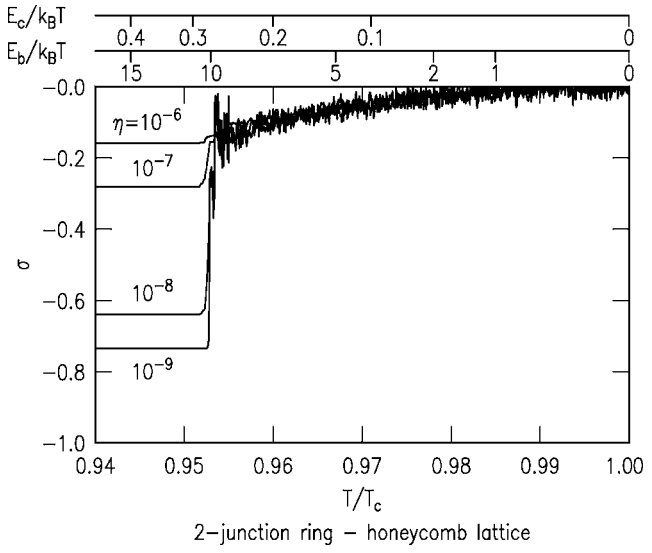

FIG. 13. Bond order as a function of reduced temperature T/T_c calculated using Monte Carlo techniques as described in the text, for various cooling rates η. Scales for the reduced barrier energy E_b/k_bT and ring-ring coupling energies E_c/k_BT are included in the top of the figure.

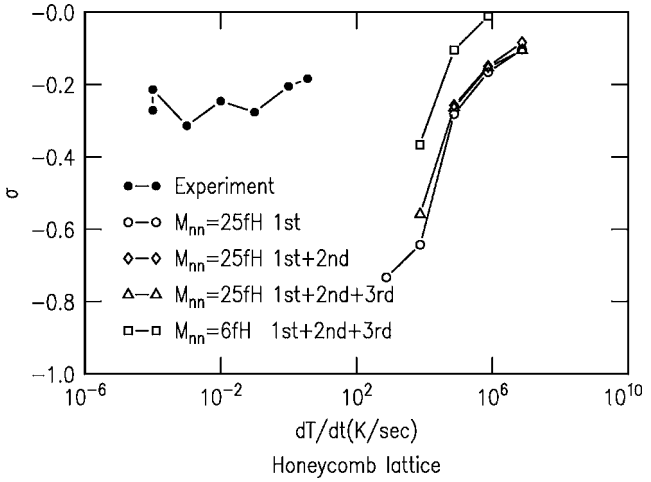

FIG. 14. Low temperature limit of the bond order, as determined experimentally with SQUID microscopy imaging (solid symbols) for the honeycomb lattice of Fig. 6, and as calculated for the same lattices using Monte Carlo techniques as described in the text (open symbols), for two values of the mutual inductance between nearest neighbor rings. The calculations labeled 1st include only nearest neighbor spin-spin coupling, those labeled 1st+2nd also include second nearest neighbors, and those labeled 1st+2nd+3rd also include third nearest neighbors.

that only a few shells of neighbors need be included in our simulations.

For simulation of the experimental cooling process, for each iteration cycle, the probability of a spin flip P_i,

$$P_i = e^{-E_{bi}/k_bT}, \tag{15}$$

is calculated for each ring. A random number between 0 and 1 is generated. If this number is less than P_i, the spin of the ring is flipped. The process is repeated throughout the array, and the temperature is gradually reduced until no more spin flips occur. Figure 13 shows results from a Monte Carlo simulation of the honeycomb lattice of Fig. 3, using the ring parameters of Table I, plotting the bond order σ as a function of the reduced temperature T/T_c, for various values of η, the change in T/T_c per iteration cycle. In this case only the 1st nearest neighbor interactions were used. As the temperature is reduced the spin flipping probabilities decrease, and antiferromagnetic ordering gradually occurs. Furthermore note that the bond order continues to change well below the estimated freezing temperature $E_b/k_bT_f \approx 8$. The effective cooling rate of the simulation is given by $dT/dt=\eta T_c/\pi\beta\tau = 7.52\times10^{11}\eta$ K s^{-1}. Therefore, the slowest cooling rate simulated is about 1×10^3 K/s, much faster than the experimental cooling rates. Although it would in principle be possible to use sufficient computer time to match the modeled cooling rates to experiment, the modeling indicates stronger anti-ferromagnetic ordering than is observed, even at these very fast cooling rates.

Figure 14 shows experimental results for the final bond order for the honeycomb array of Fig. 6, for various cooling rates. Experimentally the effect of cooling rate on final bond-order is weak. Also shown in this figure are the results of our

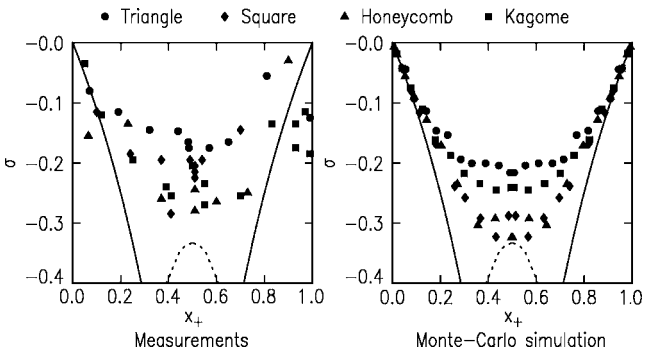

FIG. 15. (a) Measured dependence of the bond order σ upon fraction of spin-up rings x_+, for the four different types of arrays shown in Fig. 6, obtained by cooling in various fields. The solid line is the theoretical maximum negative bond order for a geometrically unfrustrated array; the dashed curve is that for a frustrated array. Some of the experimental points at very low and high x_+ fall below the theoretical maximum negative bond order because of edge effects due to the finite array sizes imaged. (b) Results of a Monte Carlo simulation of the cooling process for these arrays, as described in the text.

Monte Carlo simulations for the honeycomb array. The points labeled $M_{nn}=25fH$ use all of the parameters in the simulation as calculated following Table I. The points labeled $M_{nn}=6fH$ used a reduced value of the ring-ring mutual inductance. Also shown are curves comparing the predictions if only the nearest neighbor spin-spin interactions are included, with results if 2nd and 3rd nearest neighbors are also included. The mutual inductance between a ring and its further neighbors (e.g., 2nd nearest and 3rd nearest) is taken to be scaled by the cube of the ratio of the relevant center-to-center distances. Qualitatively, the inclusion of next nearest neighbors reduces the tendency towards anti-ferromagnetic ordering. However, it appears that the inclusion of 3rd nearest neighbors does not change the results much further. Similarly, reducing the strength of the spin-spin coupling by a factor of 4 also reduces the tendency to order. However, in all cases it appears that if the simulation were to be extended to sufficiently slow cooling rates to match experiment, ordering beyond a few lattice sites would result.

This failure of our arrays to order implies that there is a source of disorder that we have not taken into account properly. There are three additional sources of disorder that we have considered. The first is a distribution in Nb critical temperatures, and the second is a distribution in junction critical currents. In each case, our simulations indicate that an unrealistically large distribution width is required to significantly effect the predicted final σ value versus cooling rate curves. In all the cases we have explored numerically: Reducing E_b, reducing E_c, increasing the width of the T_c distribution, or increasing the width of the I_c distribution, the σ versus cooling rate curves can be shifted vertically in Fig. 15, but the slope of these plots does not change qualitatively. Further, the predicted final values for σ are relatively insensitive to a finite distribution width. For example, a flat random distribution of either the junction critical currents I_c or the ring self-inductances L with a 20% full width, using the parameters of Fig. 13, with $\eta=10^{-7}$, results in a change of the predicted final state σ from -0.28 to -0.26. We estimate that the distribution width of our junction critical currents and that of the ring hole sizes were much less that 10%, over the typical field of view of Figs. 6(a)–6(d). The ring self-inductances should be roughly proportional to the hole sizes. A final factor that might inhibit ordering of our arrays is if the cooling rate is not uniform. However, inspection of Fig. 13 indicates that fast jumps in temperature larger than $0.001T_c \approx 10$ mK would be required to significantly affect the final bond-orders. It seems unlikely that our temperature sweeps are that nonuniform. It is, therefore, difficult to see how the experimental data can be fit using the present simulations, and some factor that we have not considered correctly is causing the failure of our arrays to achieve order beyond a few lattice sites.

Nevertheless, the experimentally determined values for the bond-order σ can be modeled fairly well, if one uses the cooling rate as a fitting parameter. The left-hand panel of Fig. 15(a) summarizes cooling experiments for all of the 2D arrays of Fig. 6. These data were taken after cooling the arrays at rates between 1 and 10 mK/s. Although anti-ferromagnetic order beyond a few lattice sites was not observed in these arrays, they did show strong anti-ferromagnetic correlations, as evidenced by the large negative bond orders. Note that there are no qualitative differences between the geometrically frustrated and nonfrustrated lattices in their tendency to anti-ferromagnetically order. For comparison, the O-rings of Refs. 1 and 6 never showed bond-orders more negative than $\sigma=-0.2$, whereas our π-ring arrays attained bond orders as negative as $\sigma=-0.3$. The right hand panel shows the results of Monte Carlo simulations for these arrays, using the ring parameters in Table I but with a cooling rate $\eta=10^{-7}$, corresponding to 7.5×10^4 K/s. In both panels the ideal curve for an unfrustrated lattice (solid line) and a frustrated lattice (dashed line) are also indicated. The experimental results can be qualitatively modeled assuming a cooling rate 10^7 times faster than the experiment.

V. CONCLUSIONS

We have shown that it is possible to use large arrays of photolithographically patterned π-rings as an analog spin system. Half-fluxon Josephson vortices in electrically connected $0-\pi$ zigzag facetted junctions order with strongly anti-parallel half-fluxon vortices through the superconducting order parameter phase. Electrically isolated 1D and 2D arrays order much less strongly. The 2D π-ring arrays show stronger anti-ferromagnetic correlations than reported previously for O-ring arrays, but not order beyond a few lattice constants. We can understand the anti-parallel phase coupling of the zigzag junctions by solving the Sine-Gordon equations. Although some features of the ordering in the 2D arrays can be understood using Monte Carlo simulations, unrealistic parameters must be used, and we do not understand why these arrays do not show order beyond a few lattice constants. One possibility is that our arrays correspond to a spin glass. A spin glass results from a combination of both frustration and disorder.[37,38] However, in the absence of some hidden symmetry breaking, it appears that our rings are

simply doubly degenerate. Further, qualitatively similar results are obtained for arrays with and without geometrical frustration. Our experiments with repeated cooling show that there is little fixed disorder in our arrays. Therefore, it seems unlikely that we have a spin glass, unless there is some form of frozen-in disorder that varies from cooldown to cooldown.

ACKNOWLEDGMENTS

The authors would like to thank D. H. A. Blank, R. H. Koch, K. A. Moler, G. Rijnders, and H. Rogalla for useful discussions. The authors also acknowledge the Dutch Foundations FOM and NWO for supporting this research.

[1] D. Davidovic, S. Kumar, D. H. Reich, J. Siegel, S. B. Field, R. C. Tiberio, R. Hey, and K. Ploog, Phys. Rev. Lett. **76**, 815 (1996).
[2] B. S. Deaver and W. M. Fairbank, Phys. Rev. Lett. **7**, 43 (1961).
[3] R. Doll and M. Näbauer, Phys. Rev. Lett. **7**, 51 (1961).
[4] A summary of the early literature appears in Physica B **152**, 1 (1988).
[5] L. N. Vu, M. S. Wistrom, and D. J. van Harlingen, Appl. Phys. Lett. **63**, 1693 (1993).
[6] D. Davidovic, S. Kumar, D. H. Reich, J. Siegel, S. B. Field, R. C. Tiberio, R. Hey, and K. Ploog, Phys. Rev. B **55**, 6518 (1997).
[7] W. Lenz, Phys. Z. **21**, 613 (1920).
[8] E. Ising, Z. Phys. **31**, 253 (1925).
[9] L. N. Bulaevskii, V. V. Kuzii, and A. A. Sobyanin, JETP Lett. **25**, 290 (1977).
[10] V. B. Geshkenbein and A. I. Larkin, JETP Lett. **43**, 395 (1986).
[11] V. B. Geshkenbein, A. I. Larkin, and A. Barone, Phys. Rev. B **36**, 235 (1987).
[12] D. A. Wollman, D. J. Van Harlingen, W. C. Lee, D. M. Ginsberg, and A. J. Leggett, Phys. Rev. Lett. **71**, 2134 (1993).
[13] D. A. Brawner and H. R. Ott, Phys. Rev. B **50**, 6530 (1994).
[14] C. C. Tsuei, J. R. Kirtley, C. C. Chi, LockSee Yu-Jahnes, A. Gupta, T. Shaw, J. Z. Sun, and M. B. Ketchen, Phys. Rev. Lett. **73**, 593 (1994).
[15] A. Mathai, Y. Gim, R. C. Black, A. Amar, and F. C. Wellstood, Phys. Rev. Lett. **74**, 4523 (1994).
[16] H. J. H. Smilde, Ariando, D. H. A. Blank, G. J. Gerritsma, H. Hilgenkamp, and H. Rogalla, Phys. Rev. Lett. **88**, 057004 (2002).
[17] H. J. H. Smilde, H. Hilgenkamp, G. Rijnders, H. Rogalla, and D. H. A. Blank, Appl. Phys. Lett. **80**, 4579 (2002).
[18] A. V. Andreev, A. I. Buzdin, and R. M. Osgood, III, Phys. Rev. B **43**, 10124 (1991).
[19] V. V. Ryazanov, V. A. Oboznov, A. V. Veretennikov, and A. Yu. Rusanov, Phys. Rev. B **65**, 020501(R) (2001).
[20] A. Bauer, J. Bentner, M. Aprili, M. L. Della-Rocca, M. Reinwald, W. Wegscheider, and C. Strunk, Phys. Rev. Lett. **92**, 217001 (2004).
[21] H. Hilgenkamp, Ariando, J. H. Smilde, D. H. A. Blank, H. Rogalla, J. R. Kirtley, and C. C. Tsuei, Nature (London) **422**, 50 (2003).
[22] F. P. Rogers, Master's Thesis, MIT, Boston (1983).
[23] L. N. Vu and D. J. van Harlingen, IEEE Trans. Appl. Supercond. **3**, 1918 (1993).
[24] R. C. Black, A. Mathai, F. C. Wellstood, E. Dantsker, A. H. Miklich, D. T. Nemeth, J. J. Kingston, and J. Clarke, Appl. Phys. Lett. **62**, 2128 (1993).
[25] J. R. Kirtley, M. B. Ketchen, K. G. Stawiasz, J. Z. Sun, W. J. Gallagher, S. H. Blanton, and S. J. Wind, Appl. Phys. Lett. **66**, 1138 (1995).
[26] H. A. Bethe, Proc. R. Soc. London, Ser. A **145**, 699 (1934).
[27] J. M. Cowley, Phys. Rev. **77**, 669 (1950).
[28] To our knowledge, although similar relations appear in, e.g., Refs. 26 and 27, the optimal values for the bond order in its present form as a function of spin-up fraction first appeared in Davidović *et al.*, Ref. 1. A simple physical argument for this form appears in Ref. 6. The lines in Fig. 15, which agree with the results of Refs. 1 and 6, were generated using our Monte Carlo simulation with a large value of the ring-ring coupling energy E_c.
[29] D. Xu, S. K. Yip, and J. A. Sauls, Phys. Rev. B **51**, 16233 (1995).
[30] H. Susanto, S. A. van Gils, T. P. P. Visser, H. Ariando, H. J. H. Smilde, H. Hilgenkamp, Phys. Rev. B **68**, 104501 (2003).
[31] V. G. Kogan, J. R. Clem, and J. R. Kirtley, Phys. Rev. B **61**, 9122 (2000).
[32] J. R. Kirtley, K. A. Moler, and D. J. Scalapino, Phys. Rev. B **56**, 886 (1997).
[33] E. Goldobin, D. Koelle, and R. Kleiner, Phys. Rev. B **66**, 100508(R) (2002).
[34] E. Goldobin, D. Koelle, and R. Kleiner, Phys. Rev. B **67**, 224515 (2003).
[35] A. Zenchuk and E. Goldobin, Phys. Rev. B **69**, 024515 (2004).
[36] E. Goldobin, N. Stefanakis, D. Koelle, and R. Kleiner, Phys. Rev. B **70**, 094520 (2004).
[37] K. Binder and A. P. Young, Rev. Mod. Phys. **58**, 801 (1986).
[38] A. Ramirez, Annu. Rev. Mater. Sci. **24**, 453 (1994).
[39] R. J. Baxter, *Exactly Solved Models in Statistical Mechanics* (Academic, New York, 1982).
[40] At low temperatures the London penetration depth λ is much shorter than the size of our rings, so that the two-fold symmetry should be only weakly broken by the presence of near-neighbor rings. However near T_c λ diverges, and some additional symmetry breaking may occur.
[41] S. G. Brush, Rev. Mod. Phys. **39**, 883 (1967).
[42] J. M. Kosterlitz and D. J. Thouless, J. Phys. C **6**, 1181 (1973).
[43] K. Binder and D. W. Heeremann, *Monte Carlo Simulation in Statistical Physics—An Introduction*, 2nd ed. (Springer-Verlag, Berlin, 1992).
[44] K. Binder, Phys. Rev. Lett. **78**, 4466 (1997).
[45] N. Metropolis, A. W. Rosenbluth, M. N. Rosenbluth, A. H. Teller, and E. Teller, J. Chem. Phys. **21**, 1087 (1953).
[46] M. Creutz, Phys. Rev. Lett. **50**, 1411 (1983).
[47] M. Creutz, Ann. Phys. **167**, 62 (1986).
[48] C. D. Tesche, J. Low Temp. Phys. **44**, 119 (1981).
[49] H. J. H. Smilde, Ariando, D. H. A. Blank, H. Hilgenkamp, and H. Rogalla, Phys. Rev. B **70**, 024519 (2004).
[50] J. R. Kirtley, C. C. Tsuei, and F. Tafuri, Phys. Rev. Lett. **90**, 257001 (2003).
[51] H.-J. H. Smilde, H. Hilgenkamp, G. J. Gerritsma, D. H. A. Blank, and H. Rogalla, IEEE Trans. Appl. Supercond. **11**, 501 (2001).